NACA

RESEARCH MEMORANDUM

BASE PRESSURES MEASURED ON SEVERAL PARABOLIC-ARC BODIES OF REVOLUTION IN FREE FLIGHT AT MACH NUMBERS FROM 0.8 TO 1.4 AND AT LARGE REYNOLDS NUMBERS

By Ellis Katz and William E. Stoney, Jr.

Langley Aeronautical Laboratory
Langley Field, Va.

CLASSIFIED DOCUMENT

NATIONAL ADVISORY COMMITTEE
FOR AERONAUTICS

WASHINGTON
October 26, 1951

NATIONAL ADVISORY COMMITTEE FOR AERONAUTICS

RESEARCH MEMORANDUM

BASE PRESSURES MEASURED ON SEVERAL PARABOLIC-ARC BODIES OF REVOLUTION IN FREE FLIGHT AT MACH NUMBERS FROM 0.8 TO 1.4 AND AT LARGE REYNOLDS NUMBERS

By Ellis Katz and William E. Stoney, Jr.

SUMMARY

Base pressures were measured on several fin-stabilized bodies of parabolic-arc profile in free flight at Mach numbers from 0.8 to 1.4 and at Reynolds numbers from 20 to 130 million. The bodies varied in length from 6 to 25 diameters and had afterbodies which converged to base areas equal to 19.1 percent of the frontal areas. Pressures were also measured on the side of the bodies immediately ahead of the bases.

The following observations were noted: The base pressure coefficients varied from -0.05 to 0.02 at high-subsonic speeds, from -0.10 to 0.09 at transonic speeds, and from -0.10 to 0 at supersonic speeds, the value depending on the convergence of the afterbody. For the present parabolic afterbodies of greater length than 3 diameters, increasing the convergence had the effect of increasing the base pressure and, correspondingly, reducing the base drag. For the most convergent afterbodies, a flow compression existed at the corner of the base. The coefficients of base drag for the test bodies were low, generally less than 0.010.

INTRODUCTION

The pressure which develops over the base of a flat-ended body is of particular interest in the design of jet-powered aircraft. This pressure, which is termed base pressure, has been measured on bodies having small degrees of afterbody convergence (see reference 1, for example) and is of such magnitude as to affect seriously the performance, for certain flight conditions, of aircraft having bodies with little or no boattail. Fewer base pressure data are available, however, for bodies which have moderate-to-large degrees of afterbody convergence, particularly through the transonic speed range and at large Reynolds numbers.

[redacted]

In order to present such data, this paper reports experimental results obtained on rocket-propelled bodies at the Pilotless Aircraft Research Station at Wallops Island, Va. The parabolic-arc bodies had base areas equal to 19.1 percent of the frontal areas and were tested at Mach numbers from 0.8 to 1.4 at Reynolds numbers from 20 to 130 million. The results include pressure measurements on the bases and sides of the bodies immediately ahead of the bases as well as total body drag. The bodies varied in length from approximately 6 to 25 diameters and had stabilizing fins located forward of the bases.

SYMBOLS

C_{p_b}	coefficient of base pressure related to free-stream conditions $\left(\frac{p_b - p_o}{q_o}\right)$
C_{p_b}'	coefficient of base pressure related to local-stream conditions immediately ahead of the base $\left(\frac{p_b - p_s}{q_s}\right)$
C_{p_s}	coefficient of side pressure related to free-stream conditions $\left(\frac{p_s - p_o}{q_o}\right)$
C_D	coefficient of drag $\left(\frac{\text{Drag}}{q_o S}\right)$
C_{D_b}	coefficient of base drag $\left(-C_{p_b}\frac{S_b}{S}\right)$
p	measured pressure
q	dynamic pressure $\left(0.7M^2p\right)$
M	Mach number
r	body radius
x	body station, measured from the nose
L	total body length
D	maximum body diameter

[redacted]

S	maximum body area $\left(\pi D^2/4\right)$
$K = \frac{l}{L}$	
l	body station location of maximum diameter (referenced to nose)
$\frac{l}{D}$	forebody length, diameters
$\frac{L - l}{D}$	afterbody length, diameters
R	Reynolds number based on body length

Subscripts:

o	conditions in free stream
s	conditions at side of body immediately ahead of the base
b	conditions on base

MODELS AND TESTS

The general arrangement of the test configurations is shown in figure 1, and photographs of the test models are shown in figure 2. The profiles of the bodies describe parabolic arcs with vertexes located at the body maximum radius. The equations defining the profiles are given below:

$$\frac{2r}{D} = 1 - \frac{1}{K^2}\left(K - \frac{x}{L}\right)^2 \qquad \text{when} \quad 0 \leqq \frac{x}{L} \leqq K$$

$$\frac{2r}{D} = 1 - \frac{0.5627}{(1 - K)^2}\left(\frac{x}{L} - K\right)^2 \qquad \text{when} \quad K \leqq \frac{x}{L} \leqq 1$$

[redacted]

The following table lists the values of the geometric parameters defining the bodies of the present test models (the models are numbered according to increasing length (in diameters) of the afterbodies - for reasons which will be apparent subsequently):

Model	$K = \frac{l}{L}$	Total L/D length (diam.)	Afterbody length, $\frac{L - l}{D}$ (diam.)	Forebody length, $\frac{l}{D}$ (diam.)
1	0.40	6.04	3.62	2.42
2	.40	8.91	5.35	3.56
3	.60	17.78	7.11	10.67
4	.40	12.50	7.50	5.00
5	.60	24.50	9.80	14.70

For all models the frontal area $(\pi D^2/4)$ was 0.307 square foot, and the base area was 0.0586 square foot. The bodies were constructed of wood and finished with clear lacquer to form a smooth and fair surface.

The test vehicles were stabilized by three duralumin fins, which were swept back 45° and had a total exposed area of 1.69 square feet. In the streamwise direction the fins had hexagonal sections of 0.0278 thickness ratio. The trailing edge of the fins intersected the bodies at the 90.53-percent station.

A two-stage propulsion system was employed utilizing a 3.25-inch rocket motor MK-7 as the sustainer unit and a 5-inch HVAR motor as the booster unit. The booster unit was stabilized by four fins and was attached to the sustainer motor by means of a nozzle-plug adapter. A photograph of a typical model-booster arrangement on the launching stand is shown in figure 3.

Drag data were obtained by tracking the models with the CW Doppler radar velocimeter unit and the NACA modified SCR-584 radar tracking unit as described in reference 2. Drag coefficients have been based on body frontal area (0.307 sq ft) and represent the total drag of the configurations including fin and interference drag.

Each model was equipped with a standard NACA two-channel telemeter for recording pressures. Pressures were measured at the base and on the

[redacted]

side of the model immediately ahead of the base for all models except model 4. The side orifice was located midway between two stabilizing fins. The base orifice was located near the rim of the rocket-motor nozzle for models 1, 2, and 4 and was located within the rocket blast tube for models 3 and 5. Schematic diagrams of the two types of pressure installations are shown in figure 4.

The errors in the Mach number, pressure-, and drag-coefficient data are probably within the values listed below. (It should be noted that the pressure data are continuously recorded with time and that the response of the system to sudden disturbances is extremely rapid; thus, abrupt variations of pressure with Mach number are accurately represented.)

M	Errors of measurement				
	M	C_D	C_{p_b}	C_{p_b}'	C_{p_s}
1.4	±0.005	±0.005	±0.008	±0.005	±0.010
1.1	±.005	±.007	±.015	±.010	±.020
.8	±.005	±.01	±.030	±.020	±.040

The range of the tests, in terms of Mach number and Reynolds number, is given in figure 5.

RESULTS AND DISCUSSION

For the present tests, the afterbody configuration is treated as the prime independent geometric variable by which the results may be systematized. Although other factors are present in these tests, consideration of their effects on base pressure leads to the conclusion that these variables may be regarded as incidental. A discussion of the limitations of this treatment is given in the appendix.

Figure 6 gives the Mach number variations of (a) base pressure coefficient C_{p_b} related to free-stream conditions, (b) base pressure coefficient C_{p_b}' related to local conditions immediately ahead of the base, and (c) side pressure coefficient C_{p_s} related to free-stream conditions.

[redacted]

Base Pressure Coefficient, C_{p_b}

The base pressure coefficients related to free-stream conditions are shown as functions of Mach number in figure 6(a) for the five test models. The base pressure coefficients vary from -0.05 to 0.02 at high-subsonic speeds, from -0.10 to 0.09 at transonic speeds, and from -0.10 to 0 at supersonic speeds.

The results indicate a consistent and systematic pattern when compared on the basis of afterbody configuration. Although afterbody length has been used as the parameter in the present paper, the data will correlate equally well with the boattail angle at the base since, for the test models, this parameter is inversely proportional to the afterbody length. Over almost the entire test range, as the afterbody becomes less convergent (that is, as the length of the afterbody increases), the absolute pressure on the base decreases (fig. 6(a)). This trend is further indicated by the results from reference 3 for a cylindrical body which may be represented as having a parabolic afterbody of zero convergence (that is, infinite length) at the approximate Reynolds numbers of the present tests. In the limit this trend is perhaps better thought of as a function of the convergence angle rather than the afterbody length since, in reality, the boundary layer on an infinite afterbody would make the base pressure equal to the free-stream pressure. The present results qualitatively agree with the tests at $M = 1.5$ reported in reference 4 for parabolic bodies at low Reynolds numbers and artifically induced turbulent-boundary layers.

The positive peaks in the variations of C_{p_b} near the speed of sound appear to be characteristic of the test models and are most marked for the models with extreme afterbody convergence.

Base Pressure Coefficient, C_{p_b}'

The base pressures, related to local-stream conditions immediately forward of the base, are shown in figure 6(b) as functions of free-stream Mach number for four of the test models. Expressed in this form, the pressure coefficient quantitatively defines the flow over the corner of the base: positive (+) for compression and negative (-) for expansion. The results show that the flow actually compressed in passing off the rear of the body for models 1 and 2 while an expansion occurred at the base for the configurations with less afterbody convergence (models 3 and 5). The compression at the corner of the base may have been accompanied, at supersonic speeds, by a standing shock near that

point as has been evidenced for similar bodies reported in reference 4. In this connection, it is interesting to note the abrupt increase in compression near $M = 1.0$ for models 1 and 2.

Side Pressure Coefficient, C_{p_s}

The pressure on the side of the body immediately ahead of the base, related to free-stream conditions, is shown in figure 6(c) as a function of Mach number for four of the test models. Also shown in figure 6(c) is the variation of C_{p_s} for a parabolic body (of the same family as the present models) which has been reported in reference 5. The reference configuration had an extremely convergent afterbody of 1.8 diameters and a nose of 7.1 diameters.

With the exception of the reference configuration, the pressures at the side of the bodies were less than free stream throughout the supersonic speed range. The variation of side pressure with Mach number is very similar to the base pressure variations shown in figure 6(a), particularly in the range of transonic speeds. Accordingly, it appears that the reduction in base pressure on traversing from subsonic to supersonic speeds is due primarily to a corresponding reduction in the local pressure immediately ahead of the base. The positive peaks in the coefficients of side pressure C_{p_s} and base pressure C_{p_b} near the speed of sound are probably caused by a shock moving downstream and over the side orifice as supersonic speeds are attained. A similar phenomenon was noted for the test of a body reported in reference 6.

Effect of Afterbody Length

Part of the results shown in figure 6 have been cross-plotted against afterbody length in figure 7. It should be noted here that these results are applicable only for the ratio of base to maximum diameter used in the present test $\left(\frac{D_b}{D} = 0.437\right)$. Variations are shown for the side pressure coefficient C_{p_s} and base pressure coefficient C_{p_b} related to free-stream conditions, at $M = 0.9$ and $M = 1.2$. Also shown on figure 7 are base pressure coefficients for a body the same as that reported in reference 5, which have been taken from data as yet unpublished. The values of C_{p_b} for afterbodies of zero and infinite length have been obtained from the results shown in figure 6(a) for the pointed cylindrical body (the value at $M = 1.2$ is extrapolated

from those results). The results shown on figure 7 suggest a physical picture regarding the nature of the flow at the bases of the present test bodies.

The fluid which flows past the base of a slightly convergent afterbody turns in toward the axis at the corner of the base and is expanded to a lower pressure. A short distance downstream the fluid is turned almost parallel to the axis and is thus recompressed to a higher pressure. The schlieren photographs of reference 4 have indicated that, at supersonic speeds, the recompression may be located on the body surface or downstream, depending on the afterbody convergence. It would appear from inspection of figure 7 that the base and side pressures are affected as though by a recompression which gradually moves upstream as the afterbody convergence is increased.

Drag

Total and base drag coefficients are shown as a function of Mach number in figure 8 for the configurations of the present tests. Also included in figure 8 are results from flights of models identical to several of the present tests and reported in references 7 and 8. The base drag has been reduced from the base pressure data by using the relation

$$C_{D_b} = -C_{p_b}\left(\frac{d_b}{d_{max}}\right)^2 \qquad (1)$$

and by assuming that the measured pressures are representative of the average acting on the base.

The base drag represents a small part of the total drag for the test configurations, 10 percent being the maximum indicated, throughout the range of the tests. For other base to maximum diameter ratios the base drag may be a considerable portion of the total drag since both terms in the right-hand side of equation (1) increase with increasing base diameter. For a body of given maximum diameter and afterbody length, the increase in total drag coefficient caused by increasing the base diameter is somewhat opposed by a decrease in the pressure drag over the boattail. These trends suggest that, for afterbodies of given length and maximum diameter over which no flow separation occurs, there exists an optimum value of base diameter for minimum total drag.

CONCLUSIONS

Free-flight tests have been conducted on bodies of parabolic profile which varied in length from 6 to 25 diameters and had base areas equal to 19.1 percent of the body frontal areas. Within the limits of the tests, the following conclusions appear warranted:

1. The base pressure coefficients varied from -0.05 to 0.02 at high-subsonic speeds, from -0.10 to 0.09 at transonic speeds, and from -0.10 to 0 at supersonic speeds, the value depending on the convergence of the afterbody.

2. For the present parabolic afterbodies of greater than 3 diameters, increasing the convergence had the effect of increasing the base pressure and, correspondingly, reducing the base drag.

3. The flow around the corner of the base was observed to be a compression for the most convergent afterbodies.

4. The abrupt reduction in absolute pressure at the base near the speed of sound is indicated to be due to a similar reduction in the side pressure immediately ahead of the base.

5. The coefficients of base drag were low, generally less than 0.01 for the test bodies.

Langley Aeronautical Laboratory
National Advisory Committee for Aeronautics
Langley Field, Va.

APPENDIX

DISCUSSION OF ADDITIONAL FACTORS

In the preceding discussion, afterbody configuration was referred to as the prime variable of the present tests. However, additional factors were present which would tend to limit the results and conclusions drawn in these tests. A brief discussion of these factors is presented below.

Base-Maximum Area Ratio

The ratio of base to maximum frontal area for the test bodies was 0.191. For bodies of different ratio, the results may differ from the present results.

Forebody Configuration

The present base pressure results have been correlated with systematic changes in afterbody configuration. However, the geometry of the bodies of the present tests was such that the forebodies varied without relation to the afterbodies. Calculated results by the linear theory of reference 9 have indicated that, for the present bodies, the inviscid flow conditions near the base are largely affected by afterbody changes but are little affected by changes in forebody configuration. Since the flow around the corner of the base of a body is primarily a function of the local flow near the base, it would appear that forebody configuration is of little significance in the present tests, except perhaps for Reynolds number differences due to changing forebody length. The effect of Reynolds number is discussed in the following section.

Reynolds Number

The local Reynolds numbers at the base of the bodies varied by a factor of 4 between configurations. The magnitude of the Reynolds numbers would denote turbulent flow at the bases of all bodies. The results of reference 4 for boattailed bodies and of reference 1 for cylindrical bodies indicate that a large change in the Reynolds number of a turbulent flow has little effect on base pressure. Although the evidence is not conclusive, it would appear that the effect of Reynolds number variations in the present tests are small.

[redacted]

Base Orifice Location

Base pressures were measured in the rocket blast tube (after burnout) for models 3 and 5 and were measured close to the rim of the rocket nozzle for the remaining test models (see fig. 4). This difference in base orifice location may represent a random variable in the correlation of the test results. An indication of the effect of orifice location, over the transonic speed range, is provided by the results of reference 3. For open bases, such as those of the present tests, the pressure measured inside the rocket chamber was, in each case, greater than the pressure measured on the base annulus for bodies with and without boattailing. These results may partially explain the difference in base pressure between models 3 and 4 which had almost identical afterbodies but different orifice locations.

Fin Interference

The effect of sweptback fins on the base pressure is not definitely known. The results of reference 10 show that, for thin fins (0.05 thickness or less) with rectangular plan form and trailing edge located 1 chord length ahead of the base, the effect of the fins on the base pressure was negligible. Thus, while the effect of sweepback is still unknown, it seems reasonable to assume from the thinness and position of the test fins that their effect on the base pressure was small.

REFERENCES

1. Charters, A. C., and Turetsky, R. A.: Determination of Base Pressure from Free-Flight Data. Rep. No. 653, Ballistic Res. Lab., Aberdeen Proving Ground, 1948.

2. Morrow, John D., and Katz, Ellis: Flight Investigation at Mach Numbers from 0.6 to 1.7 to Determine Drag and Base Pressures on a Blunt-Trailing-Edge Airfoil and Drag of Diamond and Circular-Arc Airfoils at Zero Lift. NACA RM L50E19a, 1950.

3. Peck, Robert F.: Flight Measurements of Base Pressure on Bodies of Revolution with and without Simulated Rocket Chambers. NACA RM L50I28a, 1950.

4. Chapman, Dean R., and Perkins, Edward W.: Experimental Investigation of the Effects of Viscosity on the Drag of Bodies of Revolution at a Mach Number of 1.5. NACA RM A7A31a, 1947.

5. Stoney, William E., Jr., and Katz, Ellis: Pressure Measurements on a Sharply Converging Fuselage Afterbody with Jet On and Off at Mach Numbers from 0.8 to 1.6. NACA RM L50F06, 1950.

6. Thompson, Jim Rogers: Measurements of the Drag and Pressure Distribution on a Body of Revolution throughout Transition from Subsonic to Supersonic Speeds. NACA RM L9J27, 1950.

7. Katz, Ellis R.: Flight Investigation at High-Subsonic, Transonic, and Supersonic Speeds to Determine Zero-Lift Drag of Bodies of Revolution Having Fineness Ratio of 6.04 and Varying Positions of Maximum Diameter. NACA RM L9F02, 1949.

8. Hart, Roger G., and Katz, Ellis R.: Flight Investigations at High-Subsonic, Transonic, and Supersonic Speeds to Determine Zero-Lift Drag of Fin-Stabilized Bodies of Revolution Having Fineness Ratios of 12.5, 8.91, and 6.04 and Varying Positions of Maximum Diameter. NACA RM L9I30, 1949.

9. Von Kármán, Theodor, and Moore, Norton B.: Resistance of Slender Bodies Moving with Supersonic Velocities with Special Reference to Projectiles. Trans. A.S.M.E., vol. 54, no. 23, Dec. 15, 1932, pp. 303-310.

10. Spahr, J. Richard, and Dickey, Robert R.: Effect of Tail Surfaces on the Base Drag of a Body of Revolution at Mach Number of 1.5 and 2.0. NACA TN 2360, 1951.

[redacted]

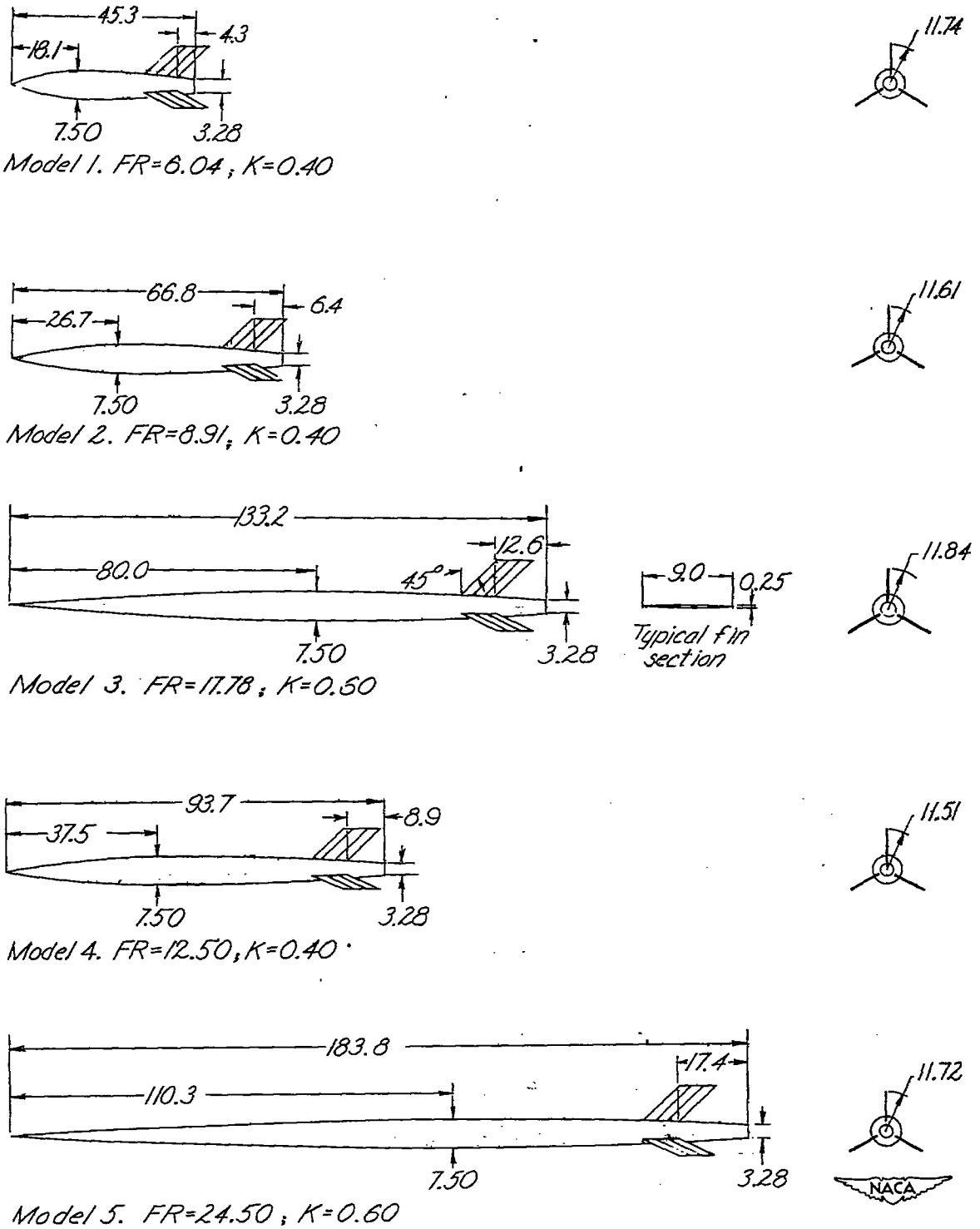

Figure 1.- General arrangements of test models. All dimensions are in inches.

[redacted]

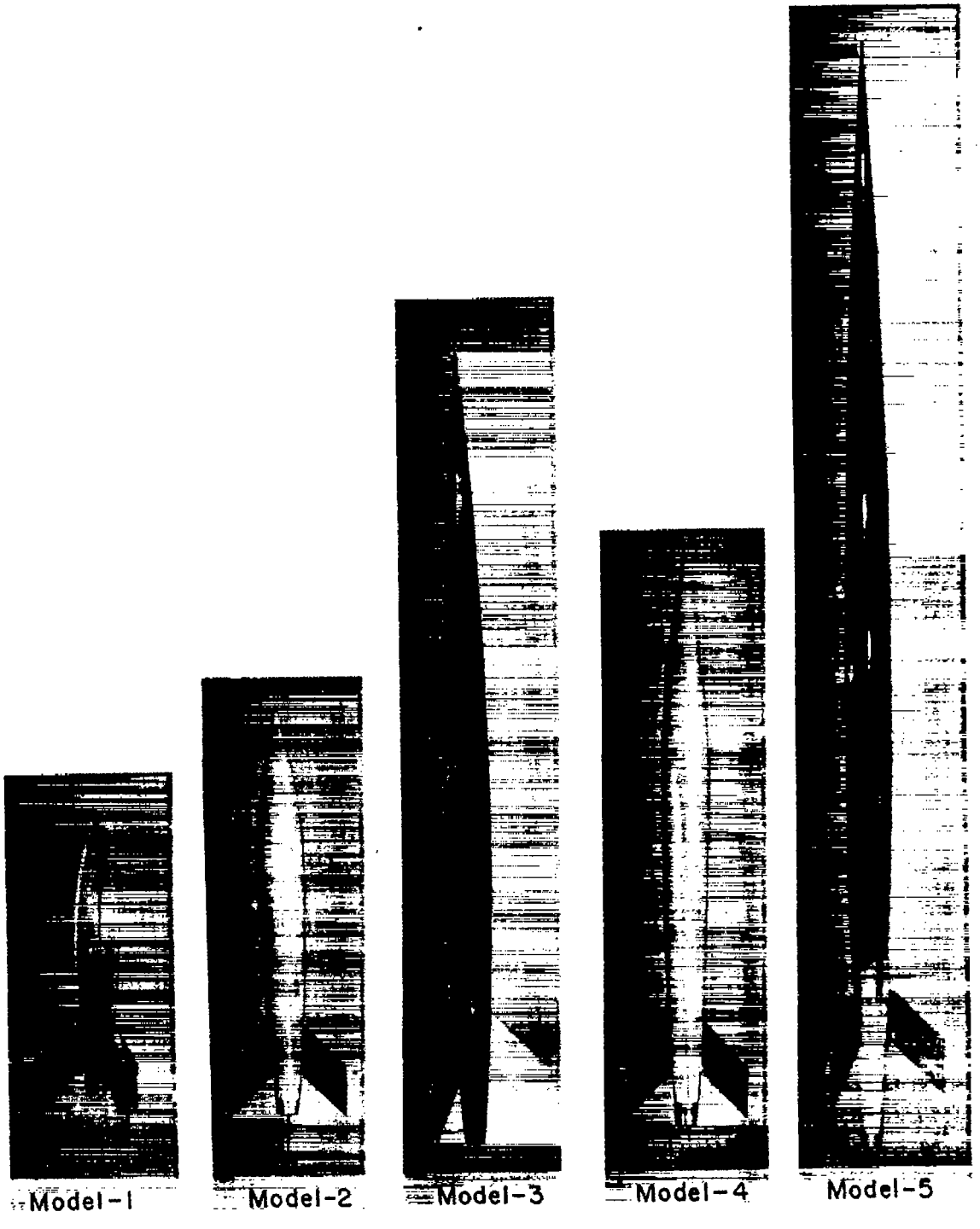

Figure 2.- General views of test models.

[redacted]

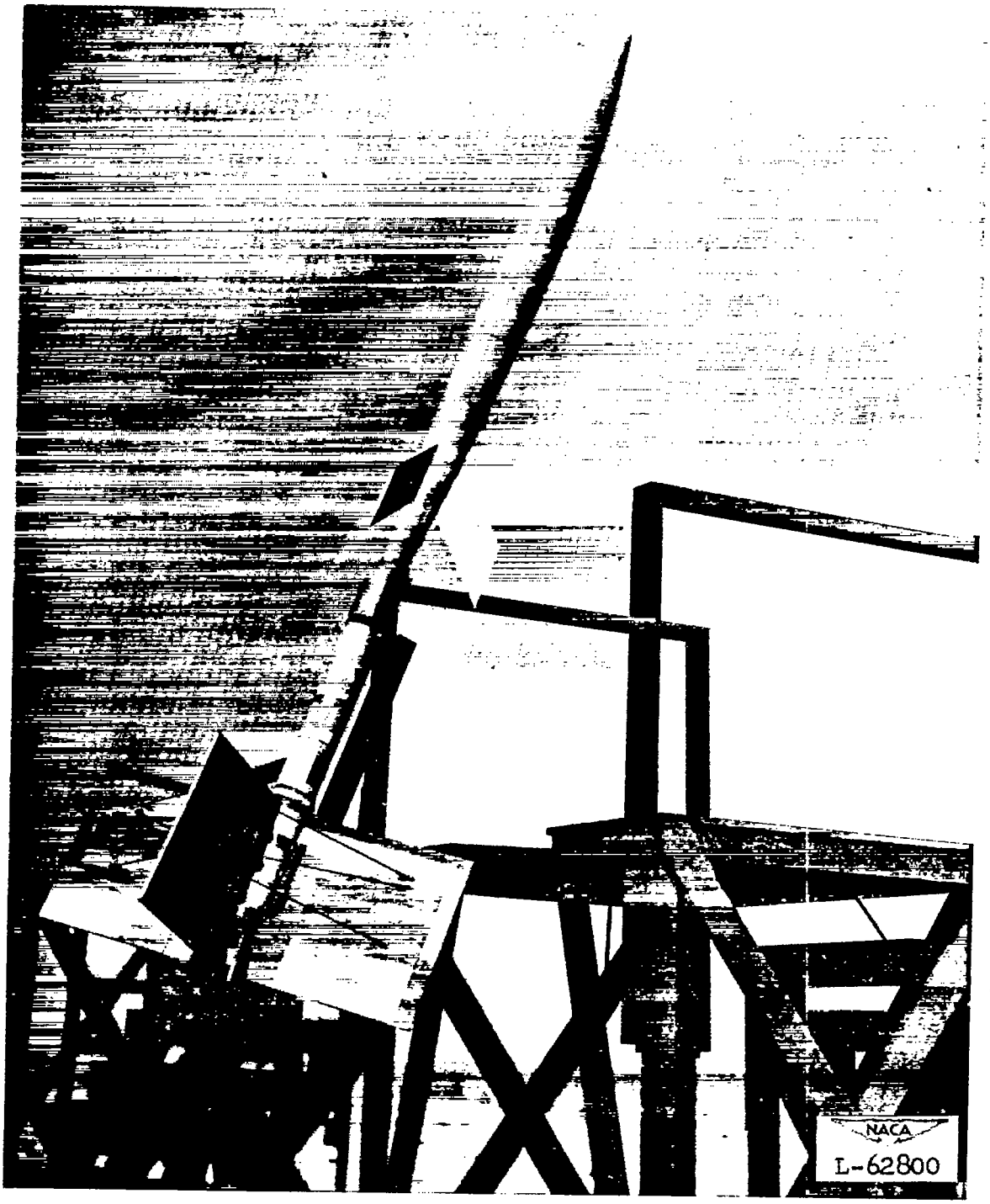

Figure 3.- Typical model-booster arrangement on launching stand.

[redacted]

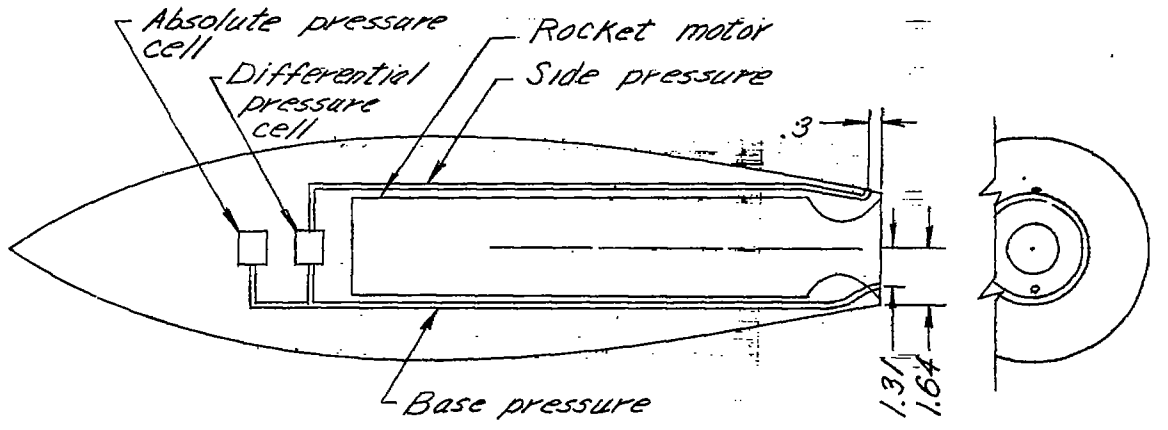

(a) System used for models 1, 2, and 4.

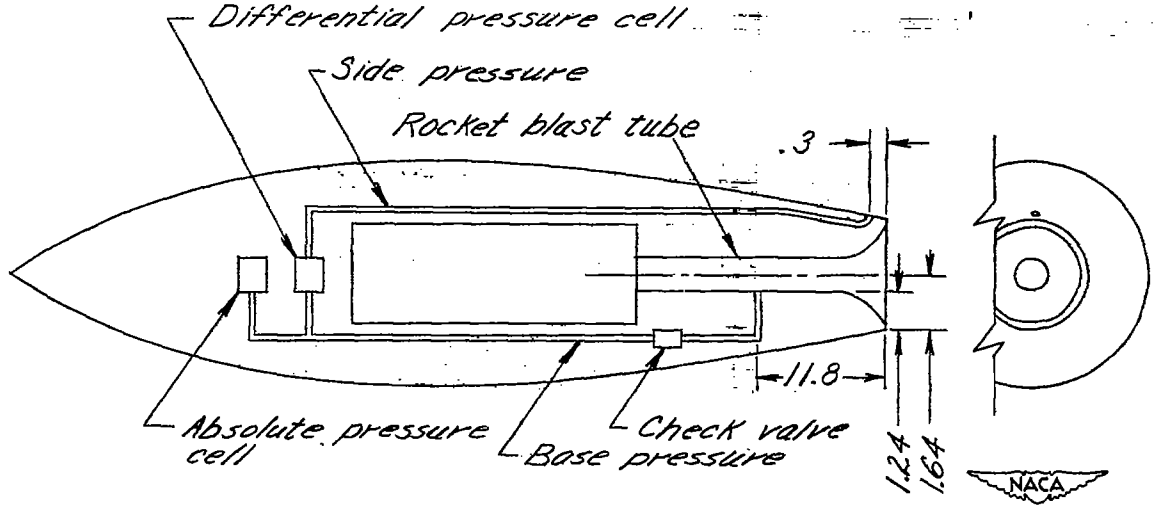

(b) System used for models 3 and 5.

Figure 4.- Schematic diagrams of pressure installations employed on test models. All pressure tubes are 0.19 inch inside diameter. All dimensions are in inches.

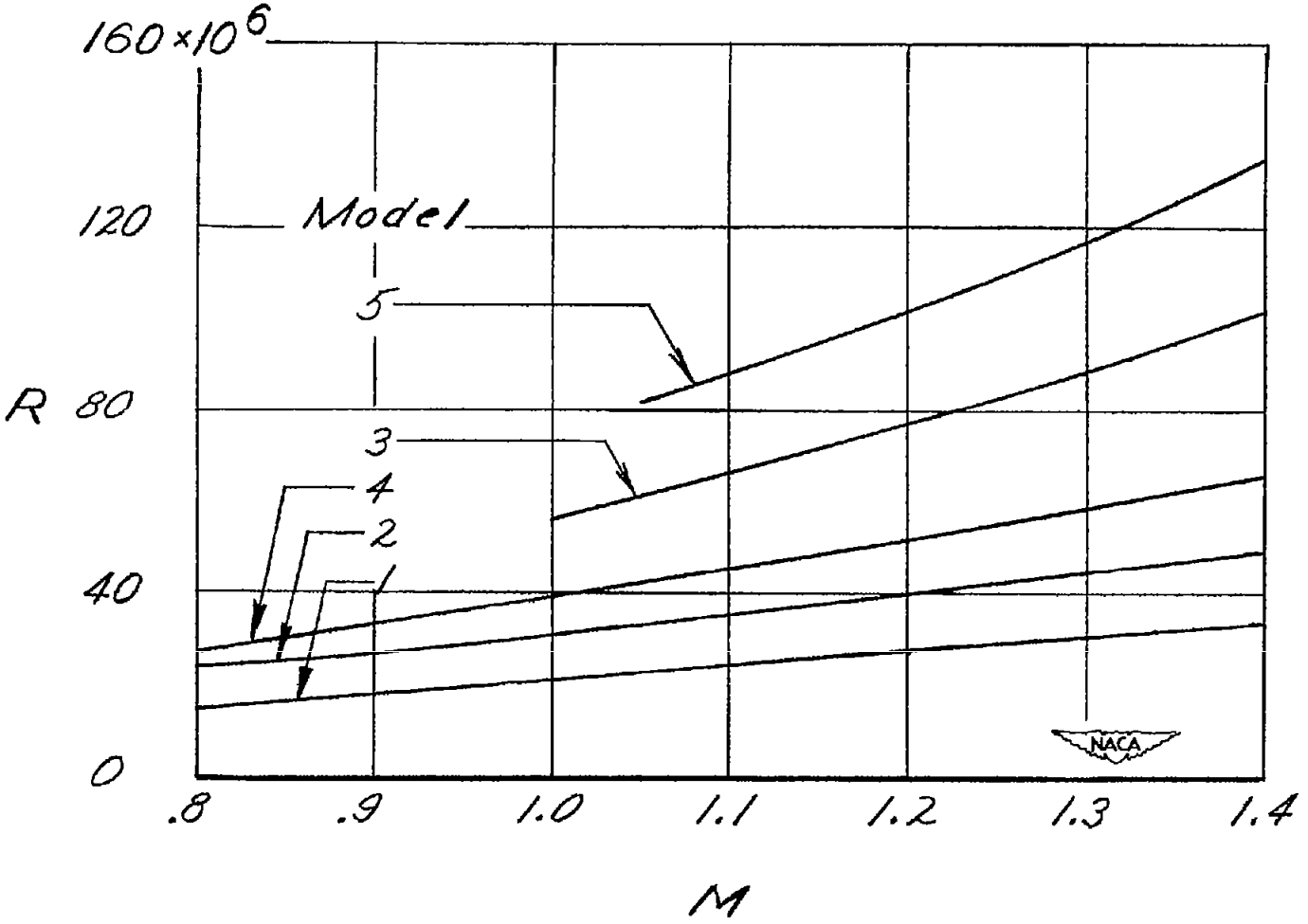

Figure 5.- Mach and Reynolds number range of test models. Reynolds number based on body length.

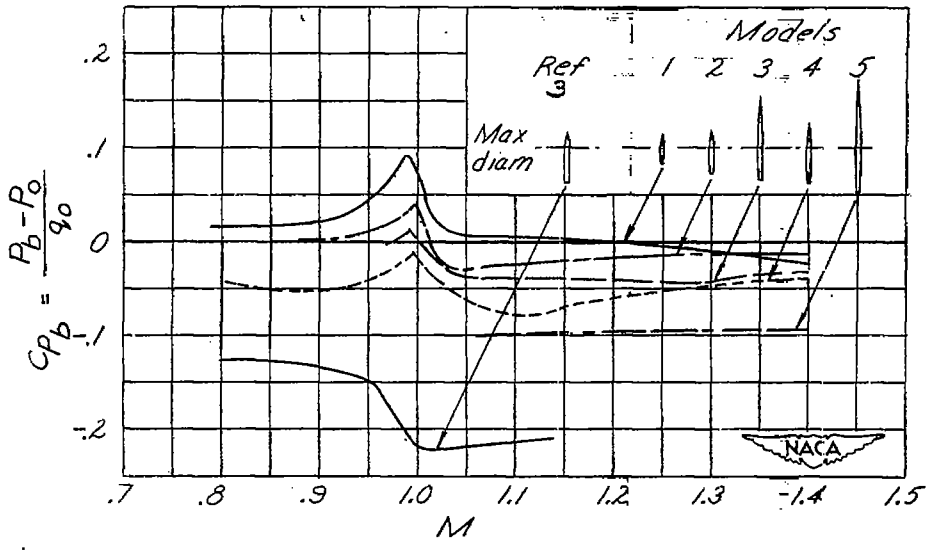

(a) Base pressure related to free-stream conditions.

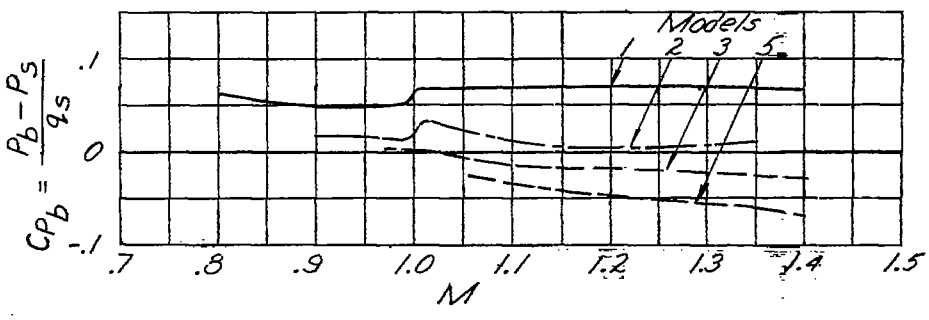

(b) Base pressure related to local-stream conditions.

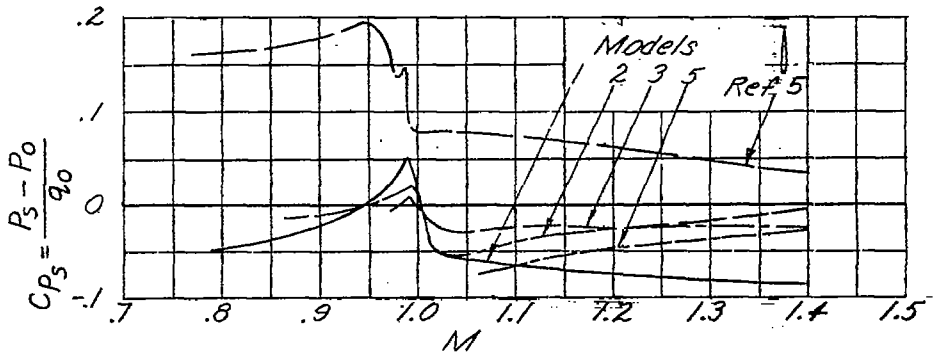

(c) Side pressure related to free-stream conditions.

Figure 6.- Pressures, in coefficient form, measured on the sides and bases of test bodies.

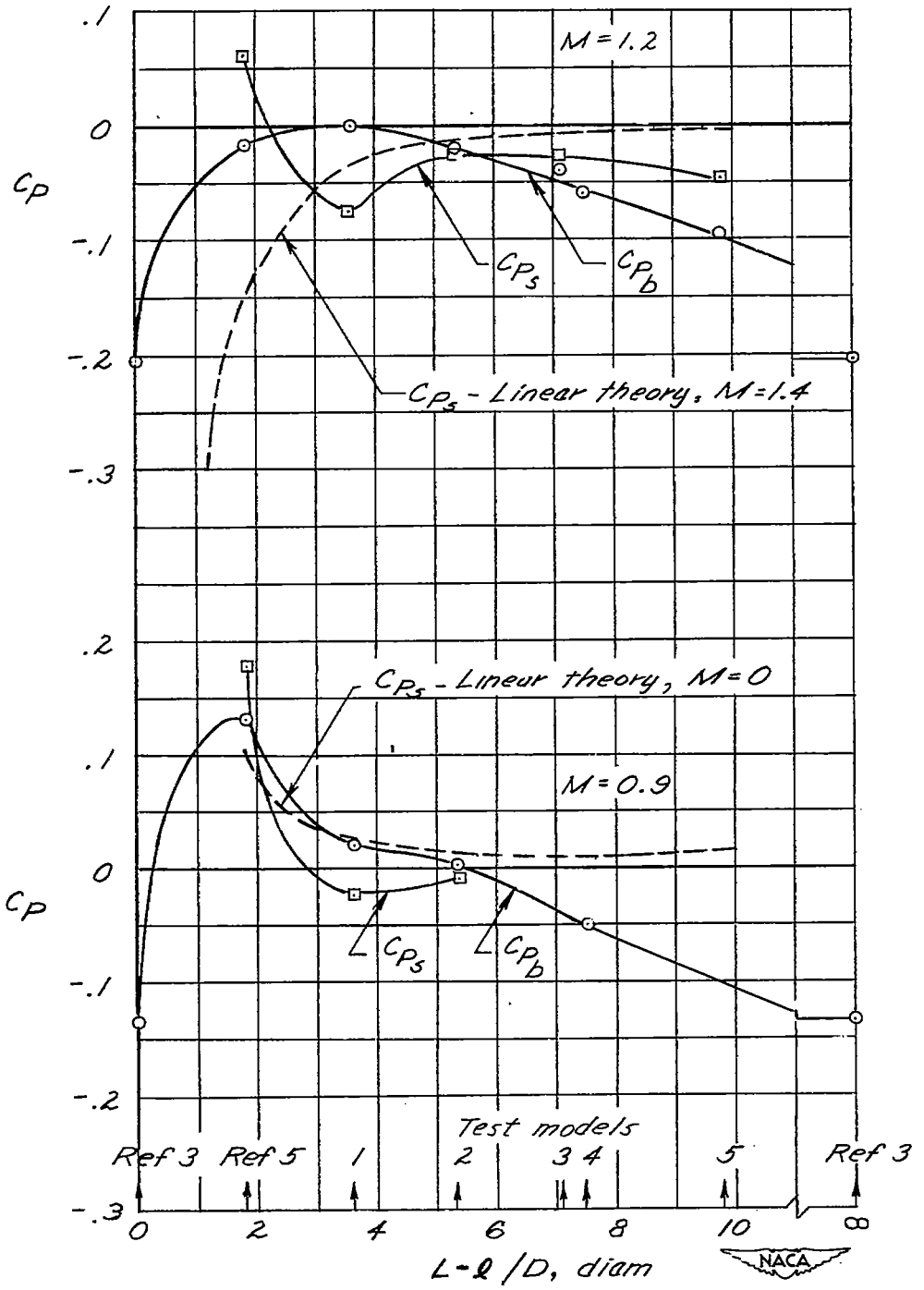

Figure 7.- Effect of afterbody length on base and side pressure coefficients for parabolic afterbodies; $\frac{d_b}{D} = 0.437$. Side pressure is measured on body surface at 99.6 percent station.

[redacted]

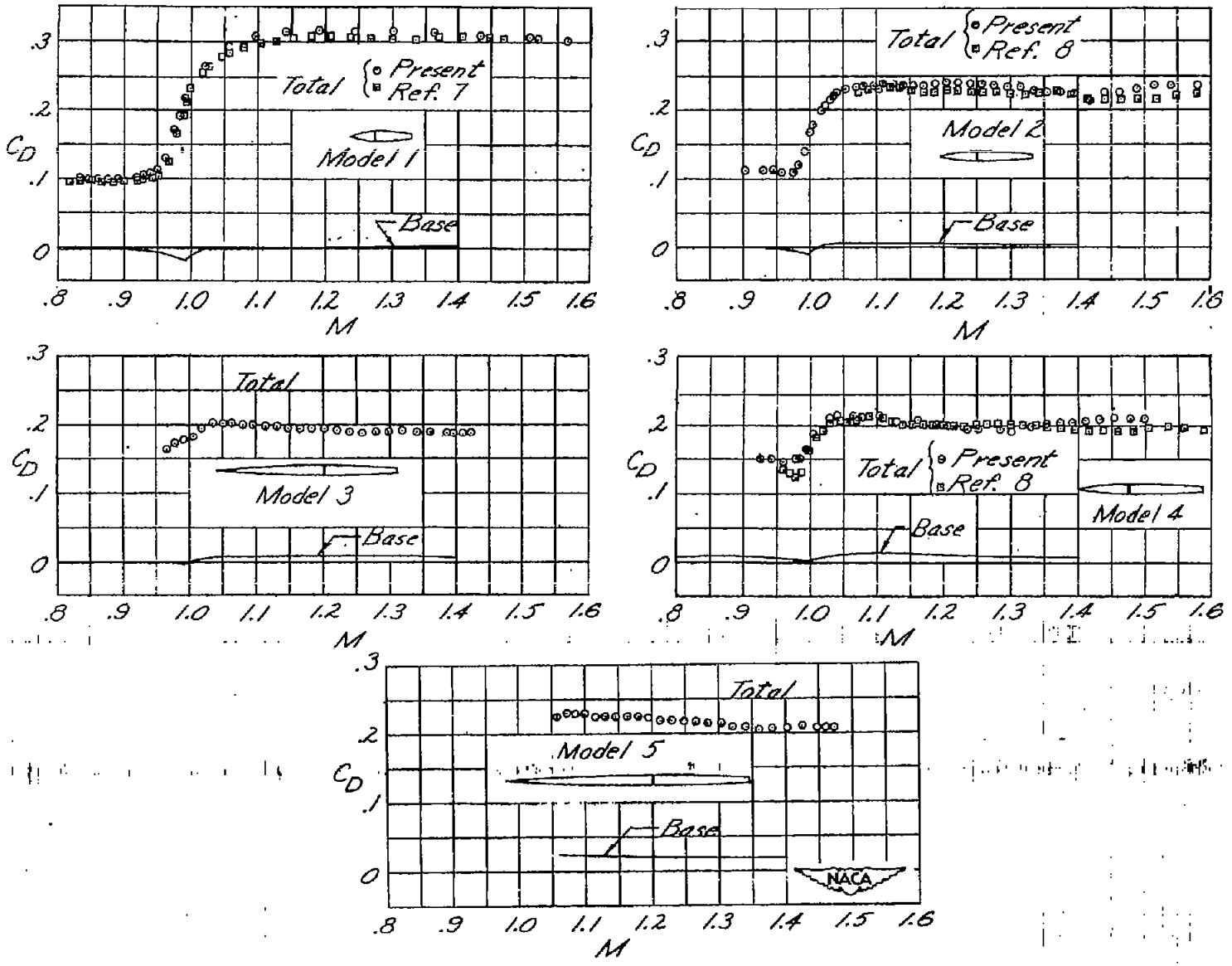

Figure 8.- Drag results for test bodies. Total drag includes drag of fins.